Preprints of the 18th IFAC World Congress
Milano (Italy) August 28 - September 2, 2011

In-Flight Results from the Drag-Free and Attitude Control of GOCE Satellite

G. Sechi*, M. Buonocore*, F. Cometto*, M. Saponara*, A. Tramutola*, B. Vinai*
G. Andrè, M. Fehringer****

** Thales Alenia Space Italia, Strada Antica di Collegno, 253 - 10146 Torino (Italy)*
(email: gianfranco.sechi@thalesaleniaspace.com
*** ESA/ESTEC, Keplerlaan 1- 2200 AG Noordwijk (The Netherlands)*

Abstract: The Gravity and steady state Ocean Circulation Explorer (GOCE) is the first Earth Explorer Core Mission of ESA's Living Planet Program. The scientific objectives of GOCE are the determination of the Earth's steady state gravity field anomalies with an accuracy of $1x10^{-5}$ m/s^2, and the determination of geoid heights with accuracy between 1 to 2 cm, at length scales down to 100 km. To meet the scientific objectives, GOCE flies in a Sun-synchronous orbit with altitude in the range 250÷280km, and it carries out two measurements: gravity gradients by the Electrostatic Gravity Gradiometer, and Precise Orbit Determination based on Global Positioning System data. An essential element for meeting the mission requirements is the Drag Free and Attitude Control (DFAC) using an ion engine for compensating the along track non-gravitational forces and a set of magnetic torquers for attitude control. The drag-free control has the task of realizing a virtual environment reducing the non-gravitational linear accelerations (from that the name *drag-free*) below a threshold compatible with the accelerometer dynamic range and with the gradiometric performance. For the same reason, the attitude control must constrain the angular accelerations and the angular rates. The mission induces requirements not only on the magnitude of the residual linear and angular accelerations, angular rate and attitude errors, but also on their spectral density in the science measurement bandwidth of [5,100] mHz. GOCE is the first European drag-free mission and the first pure magnetic attitude control system for a medium-sized Low Earth Orbit scientific satellite (about 1 ton mass). The control design has been done following already well known approaches with the introduction of customizations to cope with specific performance requirements, design simplicity and programmatic constraints. After a short presentation of the GOCE mission architecture, of the satellite and of the payload, the paper presents the main aspects of the DFAC scientific mode and its in-flight performances.

1. INTRODUCTION

The Gravity and steady state Ocean Circulation Explorer (GOCE, see Fig. 1) is the first Earth Explorer Core Mission of ESA's Living Planet Program. It was successfully launched on March 17th, 2009 with the ROCKOT Launcher from Plesetsk Cosmodrome in northern Russia.

GOCE is intended to address the shape and characteristics of Earth's gravity field with unprecedented detail. Gravity varies from place to place on the surface of Earth and in space, due to a number of factors such as Earth's rotation, position of land masses, variations in the density of Earth and the redistribution of mass due to effects such as motions of gaseous, fluid, solid components of the Earth system.

To accomplish the scientific objectives, GOCE flies in a low-altitude Sun-synchronous orbit (96.7° inclination, ascending node at 18.00h). The altitude has to be as low as possible, to maximize sensitivity to the gravity field. The design altitude range was 250÷280km.

GOCE is the first mission to employ the concept of gradiometry (Drinkwater *et al*., 2008). Its payload consists of a) an Electrostatic Gravity Gradiometer (EGG) to measure using six three-axis accelerometers the gravity gradient determined from the differential accelerations, and b) a high performance Global Positioning System (GPS) receiver providing data for Precise Orbit Determination (POD) by exploiting differential GPS techniques. A fundamental pre-requisite for the gradiometry concept is the availability of the Drag Free and Attitude Control (DFAC), designed to compensate the along track non-gravitational force using an ion engine and a set of magnetic torquers for attitude control.

2. THE SCIENTIFIC OBJECTIVES AND THE DFAC REQUIREMENTS

The scientific objectives concern both global and regional modeling of the stationary gravity field and of the geoid with high spatial resolution and high accuracy.

For the gravity field recovery, GOCE implements two measurement techniques (Allasio *et al*., 2010): (1)

measurement of the components of the gravity gradient along three spatial directions by the Electrostatic Gravity Gradiometer; (2) Precise Orbit Determination by Global Positioning System (GPS). Laser Retro-Reflectors (LRR) are present as additional payload for indepe ndent check.

Fig. 1. GOCE satellite [ESA]

The two techniques are complementary: POD allows reconstructing with high accuracy the lower harmonics of the gravity field, while the EGG provides better performance at the medium and high harmonics. The intersection is somewhere around Earth gravity field degree and order equals to 15; this leads to the definition of the Measurement Bandwidth (MBW) for the EGG, i.e., the frequency region where the measurement accuracy of the gravity gradients is maximized, from 5 to 100 mHz.

The EGG-measured signals correspond to the gradients of the components of the gravity acceleration or, in other words, to the second derivatives of the gravitational potential.

The measurement of the gravity gradients is affected by several error sources. Some of them are:

- Instrument errors, including the accelerometer noise, quantization noise, gradiometer baseline stability.
- Instrument-satellite coupling errors including mainly:
  - the coupling of the gradiometer imperfections with the residual, non gravitational, linear and angular accelerations of the satellite centre of mass;
  - the coupling of the non linear response of the accelerometers with the residual linear acceleration of the satellite.

The whole spacecraft design is driven by the need for very quiet environment. Non gravitational acceleration of the spacecraft (for example due to air drag) affects all accelerometers inside the satellite in the same manner and ideally drops out when taking differences. The common-mode acceleration is the DFAC input signal. The differential acceleration is the scientific signal. Misalignments and imperfections of the individual accelerometers cause a fraction of the common mode acceleration to leak into the differential channels.

The drag-free control has the task of reducing the non-gravitational linear accelerations below a threshold (in absolute value and in spectral density) compatible with the accelerometer dynamic range and with the gradiometric performance, when coupled to the gradiometer imperfections and accelerometer non-linearity remaining after the in-flight calibration. For the same reason, the attitude control must constrain the angular accelerations and the angular rates maximum value and stability.

DFAC implements a 4 degrees of freedom control, using ion thruster (one linear axis control) and magnetic torquers (MTR) (three axes angular controls).

The DFAC has been designed according to the specifications summarized in Table 1. Requirements are expressed both as maximum value in time and as maximum value of the one-sided spectral density inside the MBW.

Table 1. DFAC requirements for scientific observation phase

	Rotations axis	Max Value		Max one-sided spectral density inside [5,100]mHz	
Attitude w.r.t. Local Orbital Reference Frame	Roll	0.15	rad		
	Pitch	0.06	rad		
	Yaw	0.15	rad		
Angular rate w.r.t Local Orbital Reference Frame	Roll	$2\ 10^{-4}$	rad/s	10^{-5}	rad/s/√Hz
	Pitch	$0.3\ 10^{-4}$	rad/s	$5\ 10^{-7}$	rad/s/√Hz
	Yaw	$2\ 10^{-4}$	rad/s	10^{-6}	rad/s/√Hz
Angular acceleration	Roll	$1.8\ 10^{-6}$	rad/s^2	$9\ 10^{-8}$	rad/s^2/√Hz
	Pitch	$0.9\ 10^{-6}$	rad/s^2	$6.3\ 10^{-8}$	rad/s^2/√Hz
	Yaw	$0.9\ 10^{-6}$	rad/s^2	$6.3\ 10^{-8}$	rad/s^2/√Hz
Linear acceleration along track		$0.9\ 10^{-6}$	m/s^2	$2.3\ 10^{-8}$	m/s^2/√Hz

3. THE PLATFORM AND THE PAYLOAD

The satellite design was driven by aerodynamics (highly symmetric configuration; slender shape with low cross section in the flight direction; centre of pressure (COP) behind the centre of mass (COM) for passive aerodynamic stability, using winglets and trim masses), by minimization of disturbances to the measurements and by the low altitude operations. Due to the magnetic torquers based attitude control, minimization of the uncertainties in magnetic coupling between torquers, tanks and electronic equipment and magnetometer measurements played an important role.

The satellite is a cylindrical body with octagonal cross section. Design values for spacecraft dimensions, mass and inertia are shown in Table 2.

Table 2. Platform main parameters

Mass	1052 kg
Inertia matrix (begin of life)	$J = \begin{bmatrix} 174 & -16.9 & 4.48 \\ -16.9 & 2826 & 1.95 \\ 4.48 & 1.95 & 2799 \end{bmatrix}$ kgm^2
Length	5.3 m
Cross-section area	1.1 m^2
COM-COP distance	28 ÷ 31 cm

The EGG consists of three pairs of three-axis accelerometers mounted in a diamond configuration. An accelerometer pair forms a one-axis-gradiometer with 0.5m baseline. Each accelerometer can measure linear accelerations along three, nominally orthogonal, axes with acceleration noise lower than $2\cdot10^{-12}$ m/s^2/√Hz (scientific channel) and $5\cdot10^{-10}$ m/s^2/√Hz (DFAC channel).

The state-of-the-art GPS receiver designed for low-Earth orbit environment can simultaneously track 12 GPS satellites in the L1/L2 frequencies. GPS receiver provides, at 1Hz: a) C/A code range on L1; b) P(Y) code range on L1, L2; c) carrier phase on L1, L2; d) time measurement.

LRR consists of an array of symmetrically mounted corner cubes, located on the Earth-facing side of the satellite.

EGG (DFAC channel) and GPS measurement are also used in real-time by DFAC.

4. DFAC ARCHITECTURE

Besides the EGG, and GPS receiver, the DFAC sensors are:

- three autonomous star trackers (STR);
- two Digital Sun Sensors (DSS);
- six heads for the Coarse Earth Sensors and Coarse Sun Sensors, integrated in the Coarse Earth and Sun Sensors (CESS);
- three 3-axis magnetometers (MGM).

The actuators available are:

- two Ion Propulsion Assembly (IPA) units in cold-redundancy, for linear drag free control and orbit control;
- three internally redundant magnetic torquers (MTR);
- one internally redundant cold-gas thruster assembly for the gradiometer calibration Assembly (Gradiometry Calibration Assembly (GCA)).

Sensors and actuators work at different sampling frequency: EGG and IPA @ 10 Hz; STR, DSS, MGM and MTR @ 2 Hz; CESS, GPS and GCA @ 1 Hz.

To cope with the different operating phases, the DFAC has been organized in several operating modes:

- Coarse Pointing Mode (CPM). It is an acquisition mode as well as a survival mode. The main targets of CPM are satellite de-tumbling after separation, Sun acquisition and the achievement of a stable pointing.
- Extended Coarse Pointing Mode (ECPM). It improves the pointing permitting the transition to the next higher mode. It also allows orbit raising maneuvers in contingency conditions.
- Fine Pointing Mode (FPM). It is the normal operating mode providing reduced orbit decay.
- Drag-Free Mode (DFM). It is the science mode and it is structured into three sub-modes. Linear and angular acceleration controls are performed. DFM is also employed to operate the in-flight calibration of the gradiometer.

5. THE DFAC SCIENTIFIC CONTROL MODE

5.1 Drag-free linear control

The linear drag-free control is realized with a linear acceleration observer, based on a discrete-time model of the disturbances to be attenuated, and of the delay introduced by EGG DFAC channel and by ion thruster dynamics (Martella *et al.*, 2002). The observer computes real-time one-step-ahead prediction of the disturbance acceleration, by employing EGG measurements and ion thruster commanded force at current control step.

The discrete model of the plant putting in connection the commanded acceleration with measured one is (Franklin *et al.*, 1990):

$$\begin{bmatrix} x_0(i+1) \\ x_1(i+1) \\ x_2(i+1) \end{bmatrix} = \begin{bmatrix} 0 & 1 & 0 \\ 0 & 1 & 1 \\ 0 & 0 & 1 \end{bmatrix} \begin{bmatrix} x_0(i) \\ x_1(i) \\ x_2(i) \end{bmatrix} + \begin{bmatrix} \frac{1}{m} \\ 0 \\ 0 \end{bmatrix} com(i) + \begin{bmatrix} w_0(i) \\ w_1(i) \\ w_2(i) \end{bmatrix} \quad (1)$$

$$\tilde{a}(i) = \begin{bmatrix} 1 & 0 & 0 \end{bmatrix} \begin{bmatrix} x_0(i) \\ x_1(i) \\ x_2(i) \end{bmatrix} + n(i) \quad (2)$$

where:

x_0 : delayed acceleration;

x_1 : perturbing acceleration;

x_2 : first difference of the perturbing acceleration;

m : satellite mass;

com : commanded force;

w_i : process noise i;

$\tilde{a}$: measured acceleration;

n : additional measurement noise.

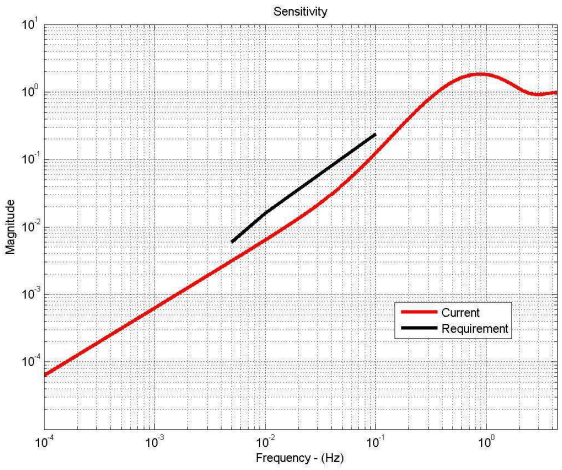

Fig. 2. Designed sensitivity function (red line) with respect to the required one (dark line)

The force command $com(i+1|i)$ to be realized by IPA at the next control step $(i+1)$ starting from the acceleration measurement received at the step (i), is obtained as follows:

$$com(i+1|i) = -m\,\hat{x}_1(i+1|i) \tag{3}$$

being $\hat{x}_1$ the estimated perturbing acceleration.

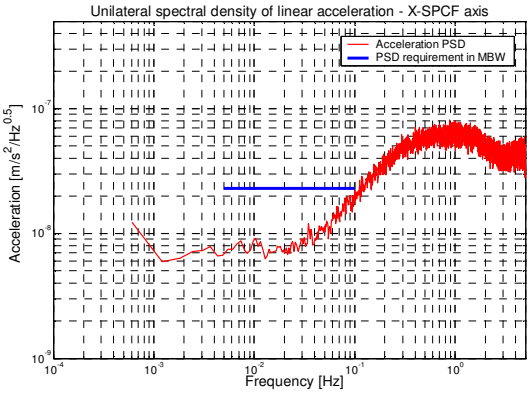

Fig. 3. One-sided spectral density of the residual linear acceleration (red line) against requirement (blue line)

The drag-free linear control sampling frequency is 10Hz. The implemented sensitivity function (Friedland *et al.*, 1986) is shown in Fig. 2: it is possible to see that the cross-over frequency is about 0.35Hz. At frequency lower than 0.01Hz, the slope is 20dB/decade; at frequency higher than 0.1Hz the slope is 40dB/decade. That slope change has been done to reduce the required IPA slew-rate.

The linear acceleration observer gains have been selected according to the pole placement approach. Fig. 3 shows the one-sided spectral density of the residual linear acceleration in the worst case condition predicted by the high fidelity simulator (E2E simulator) (Catastini *et al.*, 2003).

5.2 Attitude Control

The advantages of a fully magnetic control are a low actuation noise (fine command quantization levels are possible), high reliability and low mass. Moreover, taking advantage of the Earth Magnetic Field (EMF) magnitude at the GOCE low orbital heights, small currents are sufficient to actuate control torques.

The main problem is related to the reduced degree of controllability, because the MTR actuation system cannot produce a control torque around the EMF direction. With reference to Fig. 4, the applicable torque is only in plane π that is normal to the instantaneous EMF vector **B** ($\mathbf{T}_R$: torque required by attitude control, $\mathbf{T}_{|\mathbf{B}}$: torque component aligned with the EMF and not available, $\mathbf{T}_{\perp\mathbf{B}}$: example of possible applicable torque).

Because of the GOCE quasi polar orbit, EMF vector **B** rotates almost periodically in the orbit plane. This effect guarantees an average controllability for the roll and yaw axes with a time horizon of half an orbit. The pitch axis is always controllable. The reduced controllability leads to attitude control performances that are linked to the amplitude and phase of environmental acceleration disturbances.

Magnetic control has been widely treated in the control system literature (see for example Martel *et al.*, 1988, Psiaki *et al.*, 2001, Wisniewski *et al.*, 1996), but always with reference to small and lightweight LEO, orbiting at heights not below 450 km and without persistent platform disturbances as those due to IPA. Literature mainly provides approaches based on time varying control gains, obtaining good performances. However, the knowledge of EMF is a critical item for achieving performance and control stability.

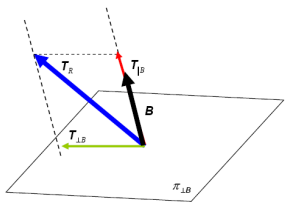

Fig. 4. Magnetic torquer applicable torque

In more recent years, Model Predictive Control (Wood et al., 2006) has been also considered, providing good results but suffering from the same limitations indicated above and requiring high computation capability (not compatible with flight on-board computer).

A constant gain solution was preferred for its simplicity and an inherent high degree of robustness. This was also driven by computational constraints imposed by on-board processor and by the wish to maintain as simple as possible the control algorithms architecture (Sechi *et al.*, 2005).

The major difficulty was related to the control law gains definition (proportional-derivative with weighted compensation of perturbing torque), taking into account the stringent requirements on angular acceleration spectral density and residual angular rate, the uneven inertia moments (ratio between roll axis and pitch/yaw axes greater than 10), magnetic cross-coupling, and the dispersion of operating conditions (air density, ion-thruster misalignment, etc.). All above points have required a smart gain selection and the modification of the transformation law from the required torque to the commanded one.

In Fig. 4, $\mathbf{T}_{\perp\mathbf{B}}$ represents one example of possible applicable torque: it is the torque on the plane π with the minimum Euclidean norm from the required one. As shown in (Arduini *et al*, 1997) and more recently in (Wood *et al.*, 2008) different allocation rule may be considered. Following a model based approach, the classical allocation rule based on the minimum Euclidean norm has been modified as follows.

In the minimum Euclidean norm allocation rule, the commanded torque is linked to the required one by:

$$\mathbf{T}_{\mathbf{C}} = \left(\mathbf{I} - \frac{\mathbf{B}\mathbf{B}^T}{\|\mathbf{B}\|^2} \right) \mathbf{T}_{\mathbf{R}} = \mathbf{B}_{tm}(\mathbf{B})\mathbf{T}_{\mathbf{R}} \tag{4}$$

By analysing the components of the 3×3 matrix $\mathbf{B}_{tm}(\mathbf{B})$, it is possible to observe how the X axis torque component of the commanded torque $T_{C,X}$ depends on the required one:

$$T_{C,X} = \left[1 - \frac{B_X^2}{\|\mathbf{B}\|^2} \quad -\frac{B_X B_Y}{\|\mathbf{B}\|^2} \quad -\frac{B_X B_Z}{\|\mathbf{B}\|^2} \right] \mathbf{T}_{\mathbf{R}}. \tag{5}$$

When the satellite flies over the Earth's equator, the EMF is mainly directed along the satellite X-axis direction, with small Y-axis component and null Z-axis component. Therefore, it is not possible to apply the desired control torque $T_{R,X}$, as $B_X^2/\|\mathbf{B}\|^2 \to 1$; instead, the control torque that is required on the pitch axis $T_{R,Y}$ affects the roll dynamics, since the product $B_X B_Y$ is not zero, and the ratio between Y-axis inertia moment and X-axis inertia moment is >15 (see Table 2). This magnetic coupling effect with uneven inertia moments have led to poor performances on roll attitude angles, angular rates and accelerations.

In order to decouple the roll and pitch axes, an ad-hoc time-varying weighting matrix $\mathbf{S}(\mathbf{B})$ has been inserted into (4) so as to pre-multiply the required torque vector $\mathbf{T}_{\mathbf{R}}$ as follows:

$$\mathbf{T}_{\mathbf{C}} = \mathbf{B}_{tm}(\mathbf{B})\left(\mathbf{S}(\mathbf{B})\mathbf{T}_{\mathbf{R}}\right) \tag{6}$$

The principle that is behind the adopted solution is to suspend any control action along the pitch axis when the roll axis is not controllable. The weighting matrix $\mathbf{S}(\mathbf{B})$ is updated at each control step considering the estimated EMF, and it is defined as

$$\mathbf{S}(\mathbf{B}) = \begin{bmatrix} 1 & 0 & 0 \\ 0 & 1-\gamma\left(\frac{B_X^2}{\|\mathbf{B}\|^2}\right) & 0 \\ 0 & 0 & 1 \end{bmatrix} \tag{7}$$

where ($0 \le \gamma \le 1$ constant weighting factor). The employment of the time-varying weighting matrix approach improves the performances on X-axis with a little worsening on Y-axis, but still meeting with margin the requirement. The use of constant gain matrices with this an ad-hoc time-varying weighting matrix has permitted to achieve performances comparable with those offered by other more complex time-varying optimal solutions (Evers, 2004).

Fig. 5 shows the one-sided spectral density of the residual angular accelerations results for two values of IPA misalignment as obtained by E2E simulator.

The stability and performance of the magnetic attitude control were the subject of a very large analysis effort. The first step of stability analysis was done by employing the classical Floquet theory (see for example Wisniewski *et al.*, 1996). The second and final conclusive validation step was done by an intensive simulation campaign of the DFAC algorithms, based on the E2E simulator. Several operating conditions were considered starting from recognized worst case and a reduced Monte Carlo analysis, providing confidence of the design robustness and performances.

The attitude control sampling frequency is 2Hz.

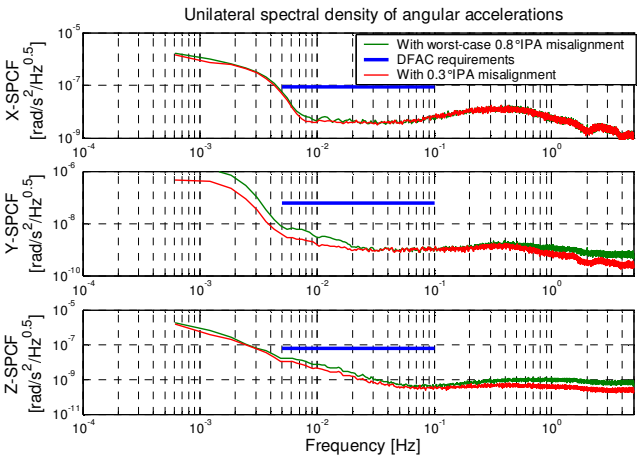

Fig. 5. One-sided spectral density of the residual angular accelerations (solid lines: 0.3° IPA misalignment, dashed lines: worst-case 0.8° IPA misalignment)

5. IN FLIGHT RESULTS OF THE DFAC SCIENTIFIC CONTROL MODE

After the launch, the successful commissioning of the spacecraft and the orbit decay phase, the scientific measurement phase officially started on September 12th 2009.

Since the beginning of the scientific phase, the DFM has been operating continuously at the mean spherical altitude equals to 259.6km (Steiger, 2011), showing results in line with or better than the expectations.

The following plots are relevant to the in-flight performance of the DFAC scientific mode. They have been obtained using the satellite telemetry: the time series are relevant to one day of data sampled at 50s, while the spectral density have been computed considering one orbit (about 5400 s) of EGG measurements sampled at 10 Hz.

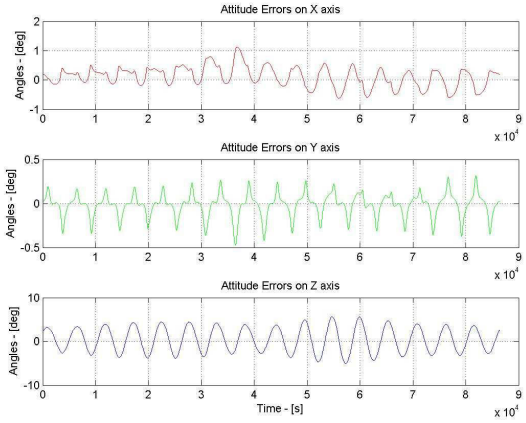

Fig. 6. Time series of attitude errors

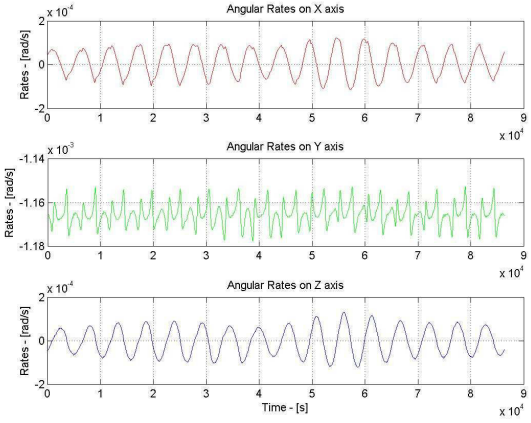

Fig. 7. Time series of angular rate

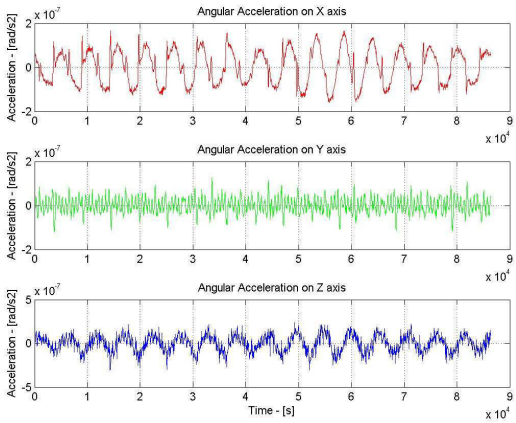

Fig. 8. Time series of angular acceleration

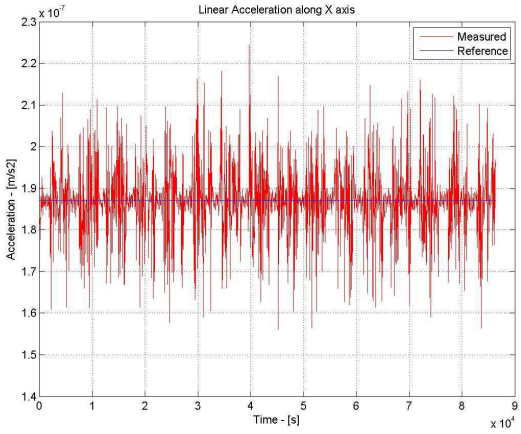

Fig. 9. Time series of linear acceleration along X axis

Fig. 6, 7, 8 and 9 show a typical behaviour of the attitude errors, angular rate, angular acceleration and linear acceleration during scientific mode. It is possible to see (in particular on X and Z rotational axis) the periodicity imposed by the magnetic field and the orbital period. Fig. 10, 11, 12 and 13 show the one-sided spectral density of the accelerations. The rows at 1Hz, 2Hz, etc. are due to the EGG thermal control (1Hz sampling frequency). Fig. 14 shows a typical profile of the commanded currents to the magnetic torquers.

Day by day, GOCE experienced different environmental disturbance levels mainly driven by the solar activity, which has a direct influence on the drag and then on the level of thrust required to counteract it. This affects mainly the angular performance in the frequency domain, because of higher induced disturbance due to IPA misalignment.

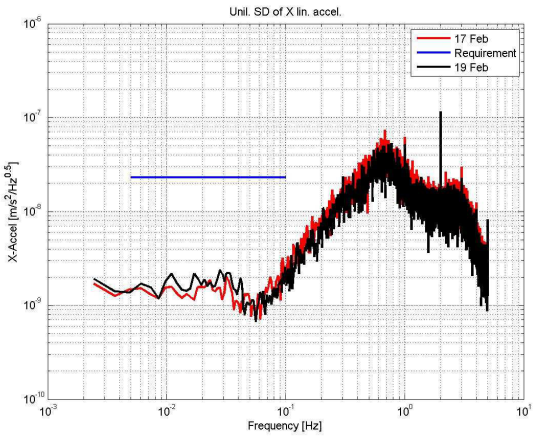

Fig. 10. One-sided spectral density of linear acceleration along X axis (red line February 17th, black line February 19th)

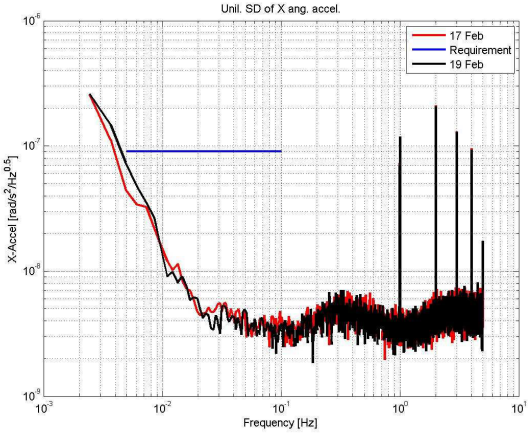

Fig. 11. One-sided spectral density of angular acceleration around X axis (red line February 17th, black line February 19th)

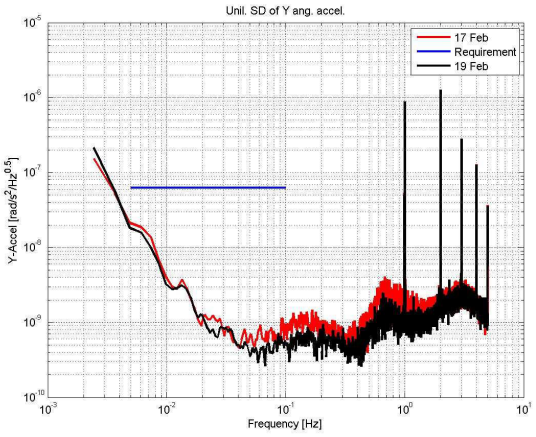

Fig. 12. One-sided spectral density of angular acceleration around Y axis (red line February 17th, black line February 19th)

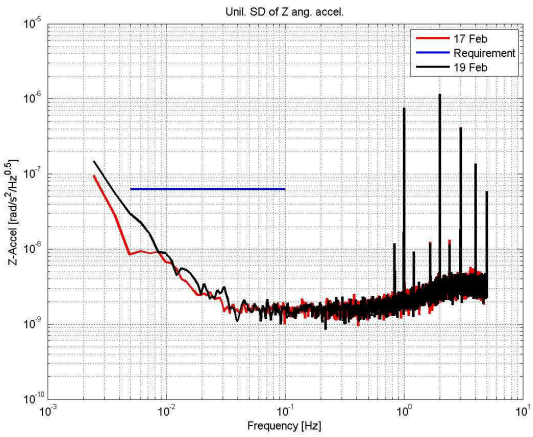

Fig. 13. One-sided spectral density of angular acceleration around Z axis (red line February 17th, black line February 19th)

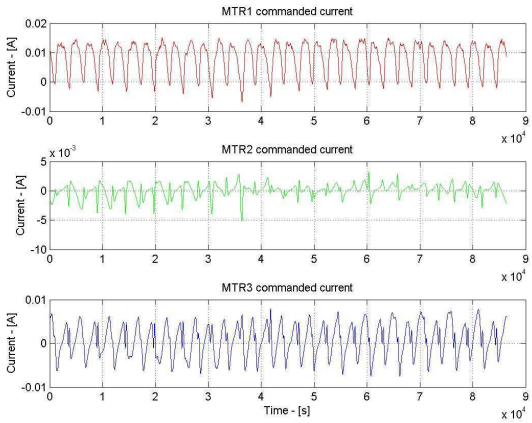

Fig. 14. Time series of commanded magnetic torquer currents

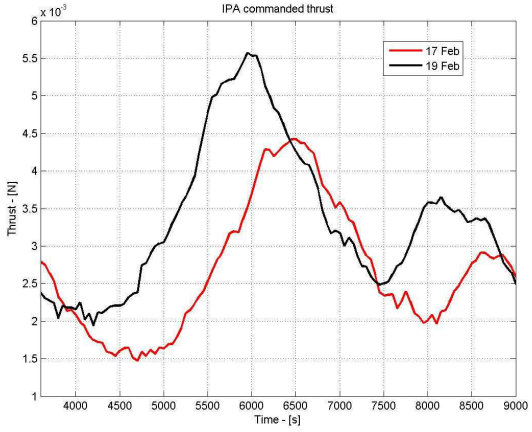

Fig. 15. Time series of commanded IPA thrust over one orbit (red line February 17th, black line February 19th)

Fig. 10, 11, 12, 13 and 15 permit to compare performance obtained in two close days (February 17th and 19th, 2011) showing extremely different solar activity. The estimated values of the mean air density were 3.0 (February 17th) and 3.6 kg/m^3 (February 19th) (values obtained using MSIS atmosphere model (Hedin)). In the comparison between the two days, the increased drag does not affect the X linear axis performance, confirming the invariance of the achieved results with respect to the change of the drag. Instead, it is possible to see that the performances at low frequency on X and Z angular axes are worse in the case the IPA thrust is, in average, higher.

5. CONCLUSIONS

The paper has presented the GOCE scientific objectives and mission, the satellite, the DFAC sub-system with special focus on scientific mode and its in-flight results.

GOCE design and development have been very ambitious and challenging, both for technologic and programmatic aspects. The gravity gradiometer, the ion thruster and the drag-free and attitude control represent a first at European level and not only. The design, the stability analysis and the assessment of the performances of the magnetic torquers based attitude control were very huge and complex activities also taking into account the unusual application (scientific mode, uneven inertia moments)

Currently GOCE is in scientific mode and the nominal mission has been extended up to the end of 2012, confirming the good health of the spacecraft and the goodness of the data provided.

ACKNOWLEDGMENT

A particular thank to Robert Harris for his useful and enlightening suggestions.

REFERENCES

A. Allasio, A. Anselmi, G. Catastini, S. Cesare, M. Dumontel, M. Saponara, G. Sechi, A. Tramutola, B. Vinai (2010), "GOCE mission: design phases and in-flight experiences", AAS-10-081, 33rd Annual AAS Guidance and Control Conference, Breckenridge, Colorado, 6-10 February.

C. Arduini, P. Baiocco (1997), "Active magnetic damping attitude control for gravity gradient stabilized spacecraft", Journal of Guidance, Control and Dynamics, Vol. 20, No. 1, January-February

G. Catastini, S. Cesare, S, de Sanctis, E. Detoma, M. Dumontel, M. Parisch, M. Saponara, G. Sechi, R. Floberghagen and D. Lamarre (2003), "The GOCE End-to-end System Simulator", 2nd Int. Workshop GOCE User Workshop, ESA-ESRIN, Frascati, Italy, 8-10 March.

M. Drinkwater, R. Haagmans, M. Kern, D. Muzi, R. Floberghagen (2008), "GOCE - Obtaining a Portrait of Earth's Most Intimate Features" ESA bulletin 133, February.

Willem-Jan Evers (2004), "GOCE dynamical analysis and Drag Free Mode control", DCT Report 2004.44, April.

G.F. Franklin, J.D. Powell, M.L. Workman (1990), "Digital Control of Dynamics Systems", Second Edition, Addison-Wesley Publishing Company

B. Friedland (1986), "Control System Design - An introduction to state-space methods", Dover publications, Inc., Mineola, New York

A. E. Hedin, "MSISE Model 1990", http://modelweb.gsfc.nasa.gov/atmos/msise.html

Martel F., Parimal K, Psiaki M. (1988), "Active Magnetic Control System for Gravity Gradient Stabilized Spacecraft", Proceedings of the Second Annual AIAA/Utah State University Conference on Small Satellites, Logan (Utah), USA, September.

Martella P., Sechi G., Canuto E. (2002) "The GOCE Drag-Free and Attitude Control Design Aspects and Expected Performances", Proceedings of the 5th International ESA Conference, Frascati, Italy, October, p. 331-338.

Psiaki M. (2001), "Magnetic Torquer Attitude Control via Asymptotic Periodic Linear Quadratic Regulation", Journal of Guidance, Control and Dynamics, Vol.24, N.2,, March-April, p.386-394.

Sechi, G., Andre, G., Andreis, D., Saponara, M. (2005) ,"Magnetic Attitude of the GOCE Satellite", Proceedings of the 6th International ESA Conference on Guidance Navigation and Control, Loutraki, Greece, 17-20 October.

C. Steiger, GO-RP-ESC-FS-6100, "Weekly operation report #106", 28 March 2011

Wisniewski R. (1996), Three-axis Satellite Attitude Control based on Magnetic Torquing – Linear Optimal Approach, in Proceedings of the 13th IFAC World Congress, San Francisco (California), USA.

M. Wood, W. Chen, D. Fertin (2006), "Model predictive control of low Earth orbiting spacecraft with magneto-torquers", Proceedings of the IEEE International Conference on Control Applications, Munich, Germany, 4-6 October.

M. Wood, W. Chen (2008), "PD control of magnetically actuated satellite with uneven inertia distribution", Proceedings of the 8th International ESA Conference on Guidance Navigation and Control, Tralee, County Kerry, Ireland, 2-5 June